# $Cs_2NaAl_{1-x}Cr_xF_6$: A family of compounds presenting magnetocaloric effect

S. S. Pedro,[1,2] J. C. G. Tedesco,[3] F. Yokaichiya,[4] P. Brandão,[5] A. M. Gomes,[6] S. Landsgesell,[7] M. J. M. Pires,[8] L. P. Sosman,[1] A. M. Mansanares,[9] M. S. Reis,[1] and H. N. Bordallo[3]

[1]*Instituto de Física, Universidade do Estado do Rio de Janeiro, Rua São Francisco Xavier 524, 20559-900 Rio de Janeiro, Rio de Janeiro, Brazil*

[2]*Instituto de Física, Universidade Federal Fluminense, Avenida General Milton Tavares de Souza, 24210-346 Niterói, Rio de Janeiro, Brazil*

[3]*Niels Bohr Institute, University of Copenhagen, Universitetsparken 5, 2100 Copenhagen, Denmark*

[4]*Instituto de Pesquisas Energéticas e Nucleares, Avenida Lineu Prestes 2242, São Paulo, São Paulo, Brazil*

[5]*CICECO and Chemistry Department, Universidade de Aveiro, Aveiro, Portugal*

[6]*Instituto de Física, Universidade Federal do Rio de Janeiro, P.O. Box 68528, Rio de Janeiro, Rio de Janeiro, Brazil*

[7]*Helmholtz Zentrum Berlin, Hahn-Meitner Platz 1, 14109 Berlin, Germany*

[8]*Instituto de Ciência e Tecnologia - ICT, Universidade Federal dos Vales do Jequitinhonha e Mucuri, Diamantina, Minas Gerais, Brazil*

[9]*Instituto de Física Gleb Wataghin, Universidade Estadual de Campinas, Caixa Postal 6165, Campinas, São Paulo, Brazil*

(Received 9 April 2014; revised manuscript received 25 June 2014; published 7 August 2014)

In this paper we explore the magnetocaloric effect (MCE) of chromium-doped elpasolite $Cs_2NaAl_{1-x}Cr_xF_6$ ($x = 0.01$ and 0.62) single crystals. Magnetization and heat capacity data show the magnetocaloric potentials to be comparable to those of garnets, perovskites, and other fluorides, producing magnetic entropy changes of 0.5 J/kg K ($x = 0.01$) and 11 J/kg K ($x = 0.62$), and corresponding adiabatic temperature changes of 4 and 8 K, respectively. These values are for a magnetic field change of 50 kOe at a temperature around 3 K. A clear Schottky anomaly below 10 K, which becomes more apparent when an external magnetic field is applied, was observed and related to the splitting of the $Cr^{3+}$ energy levels. These results hint at a new family of materials with potential wide use in cryorefrigeration.

DOI: 10.1103/PhysRevB.90.064407 PACS number(s): 75.30.Sg

Magnetic refrigerators are promising devices based on the magnetocaloric effect (MCE), with applications including hydrogen liquefiers, high-speed computers, and superconducting quantum interference device (SQUID) cooling. Thus, the quest for new materials which exhibit the MCE and promise technological improvement has attracted much attention in recent years [1–4]. Two important thermodynamic quantities characterize the MCE: the temperature change in an adiabatic process ($\Delta T_{ad}$) and the entropy change in an isothermal process ($\Delta S_T$) upon magnetic field variation. The latter is strictly related to the efficiency of a thermomagnetic cycle. The MCE is usually indirectly measured by using specific heat and magnetization data [1].

Compounds based in paramagnetic salts were used to break the 1 K barrier for the first time in magnetic refrigerators [2]. However, despite their many applications over the intervening years, the low thermal conductivity of these salts is detrimental in adiabatic demagnetization applications [5], leading to a search for new materials with MCEs at lower temperatures. Among such materials is gadolinium gallium garnet and magnetic nanocomposites based on iron-substituted gadolinium gallium garnets [6–9]. Although some of these compounds have $\Delta S_T$ values comparable to the Gd-standard material, of about 3.4 J/kg K for a field variation of $\Delta H = 10$ kOe close to room temperature [10], there are other systems that have a much larger entropy change, $\Delta S_T \approx 30$ J/kg K under $\Delta H = 50$ kOe, at 5 K, such as $Gd_3Ga_{5-x}Fe_xO_{12}$ [6]. Other successful examples consist of perovskite-type oxides [11], metal-organic frameworks containing gadolinium [12], and molecular nanomagnets, such as $Mn_{32}$ [13] and $Fe_{14}$ [14]. However, very few studies have so far reported on caloric effects in fluoride systems [15–17], which is the aim of this paper.

From the point of view of optical and structural properties, $Cs_2NaAl_{1-x}Cr_xF_6$ elpasolite single crystals, which crystallize in the $R\bar{3}m$ space group, have been thoroughly investigated [18–27]. The choice of the $Cr^{3+}$ ion as a doping impurity is justified by the fact that its $3d$ unfilled shell produces electronic transitions that increase the luminescent properties and the quantum yield of the material [20,27–29].

In this paper, we show the magnetocaloric potentials ($\Delta T_{ad}$ and $\Delta S_T$) in $Cs_2NaAl_{1-x}Cr_xF_6$ ($x = 0.01$ and 0.62) single crystals. Single crystal x-ray diffraction studies were performed and confirm the crystallographic parameters, along with EPR results to verify the local distortion caused by the $Cr^{3+}$ doping that occupies two nonequivalent octahedral sites. Magnetic susceptibility and specific heat measurements as a function of temperature and applied magnetic field bring about an interesting Schottky-like anomaly at low temperatures under an applied magnetic field. From these data, we show that the $\Delta T_{ad}$ and $\Delta S_T$ of these materials are comparable to those of some well known garnets and perovskite compounds, opening new doors for their application in cryorefrigeration.

$Cs_2NaAl_{1-x}Cr_xF_6$ single crystal samples of about $3 \times 2 \times 1$ mm$^3$ containing $x = 0.01$ and 0.62 of $Cr^{3+}$ doping were grown by hydrothermal techniques, using the temperature gradient method [20]. Single crystal x-ray diffraction data of the samples were collected on a Bruker Apex II CCD-based diffractometer using graphite monochromatized Mo-$K\alpha$ radiation. We also performed neutron activation analysis experiments on the $x = 0.62$ sample in order to check its composition. EPR measurements on the $x = 0.01$ sample were performed in a commercial Varian E-12 spectrometer. Data were obtained in the X band at room temperature. Magnetization curves vs temperature at 1 kOe and vs applied magnetic

 

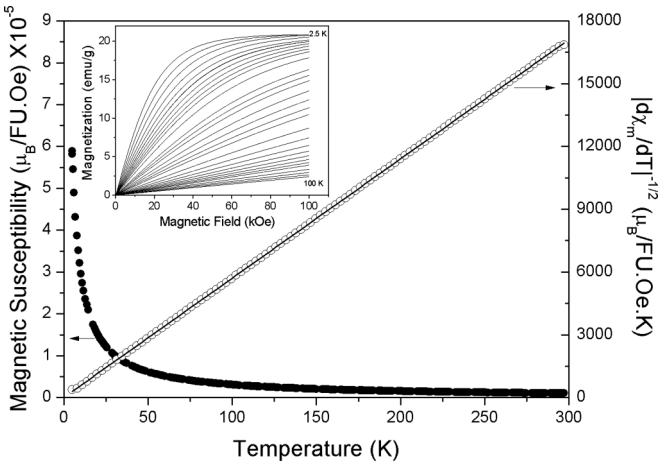


FIG. 1. Magnetic susceptibility (black circles) at 1 kOe and $|d\chi/dT|^{-1/2}$ (white circles) for $Cs_2NaAl_{1-x}Cr_xF_6$ doped with $x = 0.62$. The continuous black line is the linear fitting of $|d\chi/dT|^{-1/2}$ data. The inset shows the isothermal magnetization data, in the 2.5–100 K temperature range at magnetic field up to 100 kOe.

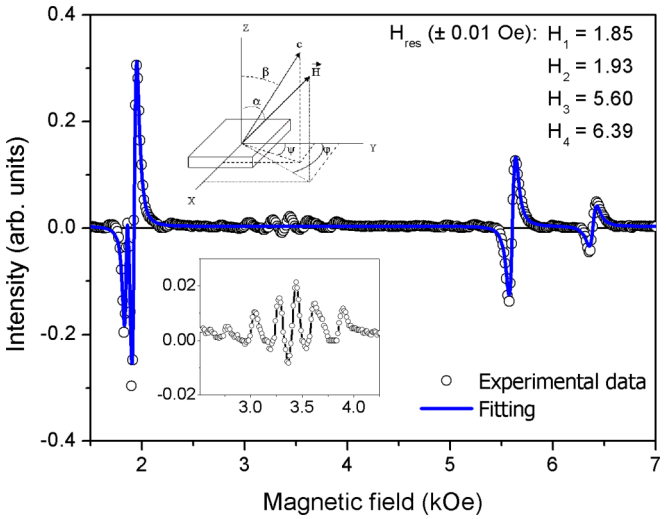


FIG. 2. (Color online) EPR spectrum obtained at $\alpha = 90^o$. The circles represent the experimental data and the blue line is the fit with Lorentzian derivatives curves. Four resonance fields were necessary for fitting. The insets show the orientation of the sample related to the crystallographic axis and the dominant face (top) and the signal from $Fe^{3+}$ contamination (bottom). This region was excluded for the fitting.

field at several temperatures were acquired using commercial Quantum Design SQUID equipment. Using a Quantum Design commercial physical properties measurement system (PPMS), heat capacity measurements with fields of 0, 50, and 100 kOe were performed with the dominant face of the sample perpendicular to the magnetic field direction.

The crystal structure of $Cs_2NaAl_{1-x}Cr_xF_6$ was verified by single crystal x-ray diffraction. For the structure refinement, it was assumed that the $Cr^{3+}$ ions are statistically distributed in the Al sites [21]. Following this procedure, the goodness of fit values were 1.166 and 1.151 for $x = 0.01$ and 0.62 samples, respectively. Both samples were found to crystallize in the rhombohedral structure previously reported for similar compounds [22,30,31]. The crystal structure contains two nonequivalent octahedral sites, where one of these sites is formed by $AlF_6$ octahedra sharing faces with two $NaF_6$ octahedra (here called S1 site), while the other site is composed of one $AlF_6$ unit sharing corners with six $NaF_6$ units (S2 site).

The magnetic susceptibility data ($\chi = M/H$) obtained for the $x = 0.62$ sample at 1 kOe and the isothermal magnetization data can be seen in Fig. 1 (with applied magnetic field perpendicular to the dominant face of the sample, defined as the one of the faces with the largest area; see the top inset in Fig. 2). In order to eliminate the temperature-independent diamagnetic contribution [32], $|d\chi/dT|^{-1/2}$ was calculated as a function of temperature. As expected for magnetically isolated ions, this response showed a Curie-Weiss behavior, and the negative paramagnetic Curie temperature extracted from fitting [$\theta_p = -0.20(4)$ K] indicates a tendency of antiferromagnetic arrangement between the $Cr^{3+}$ ions when the $Cr^{3+}$ concentration is high. The calculated effective moment also extracted from fitting was $p_{\text{eff}} = 3.90(8)$ $\mu_B/Cr^{3+}$ ion, consistent for octahedral systems containing $Cr^{3+}$ in the $S = 3/2$ spin state [$p_{\text{eff}}$ ($Cr^{3+}$) = 3.87 $\mu_B$, considering only spin] [33,34].

The magnetic susceptibility data for the $x = 0.01$ sample also obtained at 1 kOe as a function of temperature (not shown) presents a very similar behavior of the $x = 0.62$ sample. As expected for magnetically isolated ions, this response shows a Curie-Weiss behavior, with a paramagnetic Curie temperature of $\theta_p = 0.30(9)$ K and an effective moment of $p_{\text{eff}} = 5.81(3)$ $\mu_B$/dopant-ion, which is much higher than the theoretical one for systems containing $Cr^{3+}$ in the $S = 3/2$ spin state. In order to understand the high value of the effective magnetic moment, we also performed EPR measurements in this sample.

The $x = 0.01$ sample was measured at several sample positions in the resonance cavity, with which it is possible to form grouped spectra as a contour plot. The characteristics of the line splitting of these grouped central EPR spectra can be assigned to $Fe^{3+}$ impurities. In Fig. 2, which is the measurement at $\alpha = 90^o$ (where $\alpha$ is the angle between the field and the $z$ axis as shown in the inset of this figure), it is clearly displayed a signal in the magnetic field range from 2.5 to 4.5 kOe that was attributed to the presence of a $Fe^{3+}$ contamination in the sample, clear evidence that $Fe^{3+}$ and $Cr^{3+}$ occupy the same kind of site, and such behavior can be seen in some previous works on similar compounds [19,23,24,35]. In this way, the apparent discrepancy with the magnetic moment obtained from Curie-Weiss fitting from inverse susceptibility data for the $x = 0.01$ sample is accounted by the small amount of $Fe^{3+}$ impurity detected by EPR, which shows a quite high effective magnetic moment of 5.92 $\mu_B$.

The magnetic behavior of $Cs_2NaAl_{1-x}Cr_xF_6$ can be described by the Hamiltonian [35]

$$\mathcal{H} = \mu_B(\vec{H} \cdot \overleftrightarrow{g} \cdot \hat{S}) + D\left(\hat{S}_z^2 - \tfrac{1}{3}\hat{S}^2\right), \qquad (1)$$

which is characterized by two parameters: the $D$ parameter is related to the axial crystalline electric field interaction and to the contribution to the orbital momentum of the excited states, while $\overleftrightarrow{g}$ is the spectroscopic splitting tensor [36]. The resonance fields depend on the sample position relative to the

applied field and they can be simulated choosing the best set of $\overleftrightarrow{g}$ and $D$ parameters.

As indicated by single crystal x-ray diffraction results, two different sites occupied by $Cr^{3+}$ ions were considered. We could not detect anisotropy in $\overleftrightarrow{g}$, $g = g_\perp = g_\parallel = 1.95(1)$ for the S1 site and 1.97(1) for the S2 site. The $D$ parameter values for both sites were $D = -0.2540(5)\ cm^{-1}$ (for the S1 site) and $-0.3560(5)\ cm^{-1}$ (for the S2 site). By comparing our values to those reported in the literature, a reasonable agreement is found for the magnitude of this parameter [19,23–25,37]. Finally, using the transitions intensities, we obtained that 61% of $Cr^{3+}$ ions occupy the S2 site and 39% occupy the S1 site, which are close to the amount of $Al^{3+}$ in each site.

Specific heat data as a function of temperature for applied fields equal to 0, 50, and 100 kOe are shown in Fig. 3 for both samples, using a logarithmic scale for better visualization. One notices that above 10 K the magnetic field has no effect on the specific heat response, allowing us to conclude that the lattice contributions are dominant. However, if we turn to the analysis of the results with applied magnetic field for $T < 10$ K, we observe a clear increase of the signal when the field is applied. We assign this change to the manifestation of the Schottky effect, which is an anomaly related to the splitting of the energy levels of the transition metal inserted in the lattice due to crystal field [38]. Such effects are often observed in rare-earth doped materials [39], but they also can occur in systems with transition metal ions [40,41]. It is worth noticing that below 6 K the specific heat capacity increases with applied magnetic field in the interval from 0 to 50 kOe, and decreases for $H > 50$ kOe.

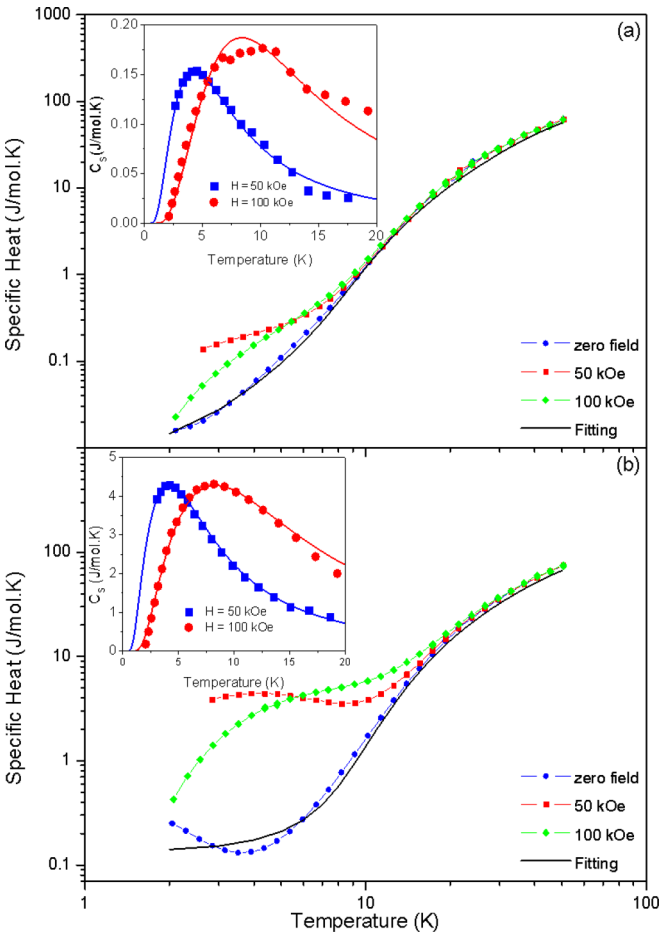


FIG. 3. (Color online) Specific heat as a function of temperature and magnetic field of the system $Cs_2NaAl_{1-x}Cr_xF_6$ doped with (a) $x = 0.01$ and (b) $x = 0.62$ of $Cr^{3+}$. Blue data were obtained at zero magnetic field, red data at 50 kOe and green data at 100 kOe. The black line is the fit obtained from zero magnetic field data, considering only the lattice contribution to the specific heat. The insets are the estimated magnetic (Schottky) contribution to the specific heat for the sample at magnetic fields of 50 kOe (blue square points) and 100 kOe (red circle points). The solid lines are the fittings corresponding to simulations of the Schottky effect.

In order to analyze and to separate the magnetic and the lattice contributions to the specific heat, we constructed a fitting routine based on specific heat data at zero magnetic field [42,43]. Two curves were generated: one considering the specific heat formulation according to the Debye theory [44], $c_D$, and the other considering the Einstein model [44], $c_E$. Although the Debye theory is more realistic than the Einstein model, the latter was also considered in the fitting procedure because it models more accurately the optical modes, while the Debye term takes better account of the acoustic modes [42]. Using only the zero-field specific heat data, a fitting was performed with a weighting factor set as a free parameter. The black line in Figs. 3(a) and 3(b) represents the theoretical fit with equation $c_{\text{latt}} = 0.65c_D + 0.35c_E$ for the $x = 0.01$ sample, while for the $x = 0.62$ sample the best-fit equation was $c_{\text{latt}} = 0.49c_D + 0.51c_E$. It can be seen that the fitting to the experimental data obtained at zero field for the $x = 0.01$ data is better than for the $x = 0.62$ data.

From the fitting procedure, the Debye ($\theta_D$) and Einstein ($\theta_E$) temperatures were also obtained, with $\theta_D = 230$ K and $\theta_E = 73$ K for the $x = 0.01$ sample, and $\theta_D = 241$ K and $\theta_E = 80$ K for the $x = 0.62$ sample. From low-temperature luminescence experiments it is known that the vibrational lines are not shifted in relation to the zero-phonon line when the doping level is increased [27], indicating that the $Cr^{3+}$ impurity concentration does not have significant influence on the lattice vibrational modes [42]. In this way, it can be seen that the difference between the values of $\theta_D$ and $\theta_E$ for both concentrations is not enough to cause a significant change in the lattice vibrational modes.

The Schottky contribution to the specific heat was obtained by subtracting the fitting curve from specific heat data obtained at nonzero fields [42]. This contribution can be seen in the insets of Fig. 3. The shape of these curves indicates a fast rise on the lower temperature side, followed by a smooth fall on the higher temperature side. Additionally, the temperature where the maximum is observed increases with applied magnetic field and doping concentration. Similar behavior has been observed in the $Ba_{8-x}Eu_xGe_{43}\square_3$ system exhibiting the Schottky anomaly at low temperatures [42].

Using the parameters obtained from EPR simulations as starting values, it was possible to obtain the energy levels for $Cr^{3+}$. The expression for the mean energy in a multilevel system at a temperature $T$ can be written as [45]

$$E = \frac{N\sum_{r=0}^{m}\varepsilon_r g_r \exp(-\varepsilon_r/k_BT)}{\sum_{r=0}^{m} g_r \exp(-\varepsilon_r/k_BT)}, \qquad (2)$$

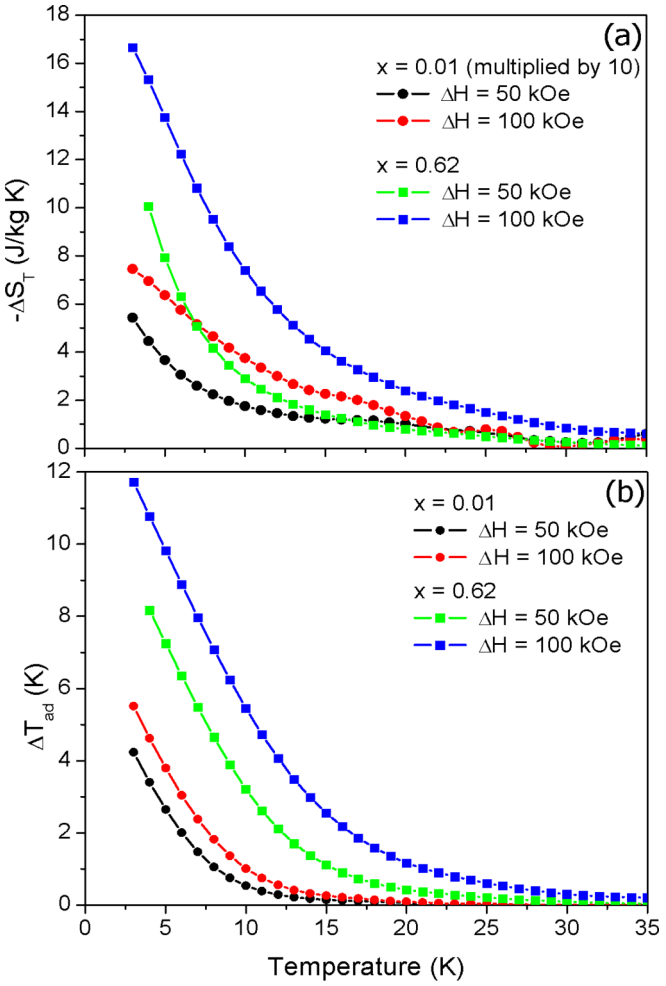


FIG. 4. (Color online) Entropy changes obtained from magnetization data (a) and temperature changes (b) of the system $Cs_2NaAl_{1-x}Cr_xF_6$ doped with $x = 0.01$ (black and red circles) and $x = 0.62$ (green and blue squares) due to variation of the magnetic field ($\Delta H = 50$ kOe and 100 kOe). For better visualization, $\Delta S_T$ for the 1% sample was multiplied by 10.

where $N$ is the number of particles in the system, and $\varepsilon_r$ and $g_r$ are the energy and the degeneracy of the $r$th level, respectively. For our system, $m = 4$. The Schottky specific heat $c_S$ was obtained by calculating $dE/dT$. The $c_S$ curves are shown in the insets of Fig. 3 as solid lines. The calculations of the values of the energy levels of $Cr^{3+}$ ions in the lattice for $x = 0.01$ sample at 300 K were useful to estimate their behavior at low temperature for both samples. We are convinced that the temperature and $Cr^{3+}$-concentration effects play a role of importance in the energy levels splitting. Concerning to $x = 0.01$ sample simulation, it was not possible to simulate the $c_S$ curves only considering the nominal $Cr^{3+}$ amount; it was necessary to add the $Fe^{3+}$ impurity, as indicated in EPR and susceptibility studies. However, as the simulations are very dependent to the dopant amount and we know only the nominal amount of $Cr^{3+}$, it was not possible to determine the amount of $Fe^{3+}$ impurity.

Of more importance is to consider that together with this anomaly, a MCE is clearly observed in this fluoride. From the well known Maxwell relations, it is possible to calculate the isothermal entropy change ($\Delta S_T$) due a variation of field ($\Delta H$) using the following expression:

$$\Delta S_T(T, \Delta H) = \int_{H1}^{H2} \left( \frac{\partial M(T,H)}{\partial T} \right)_H dH. \quad (3)$$

Moreover, as $Cs_2NaAl_{1-x}Cr_xF_6$ does not show structural phase transitions in the temperature range investigated, we can approximate this expression as a summation using the $M$ vs $H$ data [1]. Another important quantity that features in the magnitude of the MCE is the temperature change ($\Delta T_{ad}$) due to $\Delta H$, which can be obtained through the $c_p$ data as follows [1]:

$$S(T)_{H=0} = \int_0^T \frac{C(T)_{H=0}}{T} dT + S(0)_{H=0} \quad (4)$$

and

$$S(T)_{H\neq 0} = \int_0^T \frac{C(T)_{H\neq 0}}{T} dT + S(0)_{H\neq 0}, \quad (5)$$

where $S(0)_{H=0}$ and $S(0)_{H\neq 0}$ are the entropies at 0 K.

Using the $M$ vs $H$ isothermal curves data associated with the equations above, we obtained the curves shown in Fig. 4(a). It can be seen that the shape of the $\Delta S_T$ curves for both samples is very similar, with the higher magnetic field curves always having higher values, and the $\Delta S_T$ values for $x = 0.01$ sample being around ten times smaller than for the $x = 0.62$ sample. Additionally, as the temperature decreases, $\Delta S_T$ increases. The values of $\Delta S_T$ at 3 K are summarized in Table 1. These results are comparable to the values obtained for other paramagnetic fluoride systems [16,17].

Common materials that display large MCEs below 80 K are intermetallic systems such as $ErAl_2$ and $DyNi_2$, which show temperature changes of $\Delta T_{ad} \approx 10$ K (at $T = 13$ K) and $\Delta T_{ad} \approx 14$ K (at $T = 21$ K), under $\Delta H = 50$ kOe,

TABLE I. Magnetic entropy and temperature changes for $Cs_2NaAl_{1-x}Cr_xF_6$, and their comparison to other systems.

| Sample | $\Delta H$ (kOe) | $\Delta S_T$ (J/kg.K) | $\Delta T_{ad}$ (K) |
|---|---|---|---|
| $Cs_2NaAl_{0.99}Cr_{0.01}F_6$ | 50 | 0.5 | 4.2 |
| (at 3 K, this work) | 100 | 0.7 | 5.5 |
| $Cs_2NaAl_{0.38}Cr_{0.62}F_6$ | 50 | 10.0 | 8.2 |
| (at 3 K, this work) | 100 | 16.6 | 11.7 |
| Gd | 50 | 10 | 12 |
| (at 300 K) [1] | | | |
| $Gd_3Ga_5O_{12}$ | 50 | 25 | |
| (at 5 K) [6] | | | |
| $Cd_{0.9}Gd_{0.1}F_{2.1}$ | 50 | 7.2 | |
| (at 5 K) [16] | | | |
| $H_{48}C_{44}N_6O_{12}F_{45}Cr_2Gd_3$ | 50 | 22 | |
| (at 1 K) [17] | | | |
| $Gd(HCOO)_3$ | 30 | ~50 | ~20 |
| (at 1 K) [12] | | | |
| $ErAl_2$ | 50 | 37 | 10 |
| (at 13 K) [46] | | | |
| $DyNi_2$ | 50 | 21 | 8 |
| (at 21 K) [46] | | | |

respectively [46]. Turning to the analysis of $\Delta T_{ad}$ results in Fig. 4(b), the relations in Eqs. (3), (4), and (5) are equivalent for $\Delta S_T$ calculations, and Eq. (3) was used to calculate the difference $S(0)_{H=0} - S(0)_{H\neq 0}$; then we calculate the $\Delta T_{ad}$ vs T curves. It is clear that the shapes of these curves are similar to the $\Delta S_T$ curves. The results of $\Delta S_T$ using specific heat vs $T$ and $M$ vs $H$ data are in agreement [47], and these results were used to help us to estimate the entropy changes at 0 K, as we do not have specific heat data below 3 K. From $\Delta T_{ad}$ curves and the values given in Table 1, it was possible to estimate the impressive values of $\Delta T_{ad}$ obtained, which makes this material promising for future applications in magnetic refrigerator devices.

This paper shows that $Cs_2NaAl_{1-x}Cr_xF_6$ single crystals ($x = 0.01$ and 0.62) exhibit large values of temperature variation under magnetic field changes. Such an observation hints that this family of compounds is a promising material to be used in magnetic cryorefrigeration. The magnetocaloric potentials were calculated from the specific heat and magnetization measurements. The values of $\Delta S_T$ are comparable to other applied materials and the values of $\Delta T_{ad}$ are relatively large, as can be seen from Table 1.

As mentioned previously, adiabatic demagnetization of paramagnetic salts was the first method of magnetic refrigeration to reach temperatures significantly below 1 K. Although the $^3$He-$^4$He dilution refrigerator has replaced this technology in some devices, it nevertheless has the convenience of being a continuous refrigeration method, and paramagnetic refrigeration still has some advantages. A physical disadvantage of paramagnetic salts is their low thermal conductivity. Because of this limitation, paramagnetic intermetallics and other compounds (like perovskites and garnets) have been studied, and have attracted some attention with respect to their magnetocaloric properties [2]. Taking this into account together with the values of $\Delta S_T$ and $\Delta T_{ad}$ for our samples, we believe that the results found here can be an important contribution to research on magnetic refrigeration.

We thank Pedro von Ranke (UERJ, Brazil) and Walter Kalceff (UTS, Australia) for fruitful discussions. J.C.G.T.'s participation in this work was financed by the Science without Borders Program. Access to CICECO/Chemistry Department (Aveiro, Portugal), GPMR-UNICAMP (Campinas, Brazil), LMBT- UFF (Niterói, Brazil), LBT-UFRJ (Rio de Janeiro, Brazil), BERII facilities, and LaMMB MagLab (Berlin, Germany) are gratefully acknowledged by all authors. Financial support was provided by Proppi/UFF, FAPERJ, FAPESP, CAPES, CNPq, and FINEP.

[1] A. M. Tishin and Y. I. Spichkin, *The Magnetocaloric Effect and its Applications*, 1st ed., (IOP, Bristol, 2003).
[2] V. K. Pecharsky and K. A. Gschneidner, Jr., J. Magn. Mag. Mat. **200**, 44 (1999).
[3] J. R. Gómez, R. F. Garcia, A. De Miguel Catoira, and M. R. Gómez, Renew. Sustain. Energy Rev. **17**, 74 (2013).
[4] M. Schäpers, A. U. B. Wolter, S.-L. Drechsler, S. Nishimoto, K.-H. Müller, M. Abdel-Hafiez, W. Schottenhamel, B. Büchner, J. Richter, B. Ouladdiaf, M. Uhlarz, R. Beyer, Y. Skourski, J. Wosnitza, K. C. Rule, H. Ryll, B. Klemke, K. Kiefer, M. Reehuis, B. Willenberg, and S. Süllow, Phys. Rev. B **88**, 184410 (2013).
[5] F. Pobell, *Matter and Methods at Low Temperatures* (Springer, Berlin, 2007).
[6] R. D. McMichael, J. J. Ritter, and R. D. Shull, J. Appl. Phys. **73**, 6946 (1993).
[7] R. Z. Levitin, V. V. Snegirev, A. V. Kopylov, A. S. Lagutin, and A. Gerber, J. Magn. Magn. Mater. **170**, 223 (1997).
[8] R. D. Shull, R. D. McMichael, and J. J. Ritter, Nano. Mater. **2**, 205 (1993).
[9] R. D. Shull, IEEE Trans. Magn. **29**, 2614 (1993).
[10] T. Tang, K. M. Gu, Q. Q. Cao, D. H. Wang, S. Y. Zhang, and Y. W. Du, J. Magn. Magn. Mater. **222**, 110 (2000).
[11] Z. Wei, A. Chak-Tong, and D. You-Wei, Chin. Phys. B **22**, 057501 (2013).
[12] G. Lorusso, J. W. Sharples, E. Palacios, O. Roubeau, E. K. Brechin, R. Sessoli, A. Rossin, F. Tuna, E. J. L. McInnes, D. Collison, and M. Evangelisti, Adv. Mater. **25**, 4653 (2013).
[13] M. Evangelisti, A. Candini, M. Affronte, E. Pasca, L. J. de Jongh, R. T. W. Scott, and E. K. Brechin, Phys. Rev. B **79**, 104414 (2009).
[14] M. Evangelisti, A. Candini, A. Ghiri, M. Affronte, E. K. Brechin, and E. J. L. McInnes, Appl. Phys. Lett. **87**, 072504 (2005).
[15] I. N. Flerov, M. V. Gorev, A. Tressaud, and N. M. Laptash, Crystallogr. Rep. **56**, 9 (2011).
[16] A. Fernandéz, X. Bohigas, J. Tejada, E. A. Sulyanova, I. I. Buchinskaya, and B. P. Sobolev, Mater. Chem. Phys. **105**, 62 (2007).
[17] T. Birk, K. S. Pedersen, C. A. Thuesen, T. Weyhermüller, M. Shau-Magnussen, S. Piligkos, H. Weihe, S. Mossin, M. Evangelisti, and J. Bendix, Inorg. Chem. **51** (9), 5435 (2012).
[18] G. Meyer, Prog. Solid State Chem. **14**, 141 (1982).
[19] E. Fargin, B. Lestienne, and J. M. Dance, Solid State Commun. **75**, 769 (1990).
[20] L. P. Sosman, A. D. Tavares Jr., R. J. M. da Fonseca, T. Abritta and N. M. Khaidukov, Solid State Commun **114**, 661 (2000).
[21] R. J. M. Fonseca, L. P. Sosman, A. Dias Tavares, Jr, and H. N. Bordallo, J. Fluoresc. **10**, 375 (2000).
[22] H. N. Bordallo, R. W. Henning, L. P. Sosman, R. J. M. da Fonseca, A. D. Tavares, Jr, K. M. Hanif and G. F. Strouse, J. Chem. Phys. **115**, 4300 (2001).
[23] H. Vrielinck, N. M. Khaidukov, F. Callens, and P. Matthys, Radiat. Eff. Defects Solids **157**, 1155 (2002).
[24] H. Vrielinck, F. Loncke, F. Callens, P. Matthys, and N. M. Khaidukov, Phys. Rev. B **70**, 144111 (2004).
[25] H. Vrielinck, F. Loncke, F. Callens, P. Matthys and N. M. Khaidukov *et al.*, Phys. Status Solidi C **2**, 384 (2005).
[26] L. P. Sosman, F. Yokaichiya, and H. N. Bordallo, J. Magn. Magn. Mater. **321**, 2210 (2009).
[27] S. S. Pedro, L. P. Sosman, R. B. Barthem, J. C. G. Tedesco, and H. N. Bordallo, J. Luminesc. **134**, 100 (2013).

[28] G. A. Torchia, D. Schinca, N. M. Khaidukov, and J. O. Tocho, Opt. Mater. **20**, 301 (2002).
[29] S. A. Payne, W. F. Krupke, L. K. Smith, W. L. Kway, L. D. DeLoach, and J. B. Tassano, IEEE J. Quantum Elect. **28**, 1188 (1992).
[30] H. N. Bordallo, X. Wang, K. M. Hanif, G. F. Strouse, R. J. M. da Fonseca, L. P. Sosman, and A. D. Tavares, Jr., J. Phys.: Condens. Matter **14**, 12383 (2002).
[31] D. Babel and R. Haegele, Mater. Res. Bull. **8**, 1371 (1973).
[32] M. S. Reis, *Fundamentals of Magnetism* (Elsevier, New York, 2013).
[33] L. Bizo, M. Allix, H. Niu, and M. J. Rosseinsky, Adv. Func. Mater. **18**, 777 (2008).
[34] S. Coste, E. Kopnin, M. Evain, S. Jobic, C. Payen, and R. Brec, Solid State Chem. **162**, 195 (2001).
[35] J. A. Weil and J. R. Bolton, *Electron Paramagnetic Resonance: Elementary Theory and Practical Applications* (John Wiley & Sons, Hoboken, 2007).
[36] A. Abragam and B. Bleaney, *Electron Paramagnetic Ressonance of Transition Ions* (Oxford University Press, Oxford, 2012).
[37] M. G. Brik and N. M. Avram, J. Opt. Adv. Mater. **8**, 102 (2006).
[38] M. Evangelisti, F. Luis, L. J. de Jongh, and M. Affronte, J. Mater. Chem. **16**, 2534 (2006).
[39] K. Gofryk, A. B. Vorontsov, I. Vekhter, A. S. Sefat, T. Imai, E. D. Bauer, J. D. Thompson, and F. Ronning, Phys. Rev. B **83**, 064513 (2011).
[40] F. J. Lázaro, J. Bartolomé, R. Burriel, J. Pons, J. Casabó, and P. R. Nutgerem, J. Phys. Colloques **49**, C8-825 (1988).
[41] M. Affronte, F. Troiani, A. Ghirri, A. Candini, M. Evangelisti, V. Corradini, S. Carretta, P. Santini, G. Amoretti, F. Tuna, G. Timco, and R. E. P. Winpenny, J. Phys. D.: Appl. Phys. **40**, 2999 (2007).
[42] U. Khöler, R. Demchyna, S. Paschen, U. Schwarz, and F. Steglich *et al.*, Physica B **378-380**, 263 (2006).
[43] L. Xie, T. S. Su, and X. G. Li, Physica C **480**, 14 (2012).
[44] C. Kittel, *Introduction to Solid State Physics* (John Wiley & Sons, New York, 2005).
[45] E. S. R. Gopal, *Specific Heat at Low Temperatures* (Plenum, New York, 1966).
[46] P. J. von Ranke, V. K. Pecharsky, and K. A. Gschneidner, Phys. Rev. B **58**, 12110 (1998).
[47] A. Magnus G. Carvalho, A. A. Coelho, P. J. von Ranke, and C. S. Alves, J. Alloys Compd. **509**, 3452 (2011).